


Cite this: *RSC Adv.*, 2017, 7, 24885Received 30th March 2017  
Accepted 24th April 2017

DOI: 10.1039/c7ra03698a

rsc.li/rsc-advances

## Pd/APTPOSS@KCC-1 as a new and efficient support catalyst for C–H activation

Seyed Mohsen Sadeghzadeh, \* Rahele Zhiani and Shokufe Emrani

In this study, fibrous nanosilica (KCC-1) was functionalized with octakis[3-(3-aminopropyltriethoxysilane) propyl]octasilsesquioxane (APTPOSS) groups acting as the strong performers so that the palladium nanoparticles (Pd NPs) were well-dispersed on the fibers of the KCC-1 microspheres. The synthesized Pd/APTPOSS@KCC-1 nanocatalyst exhibited excellent catalytic activity for one-pot new C–H activation.

### Introduction

Benzo[*c*]pyrazolo[1,2-*a*]cinnolin-1-ones have attracted considerable research interest due to their potential as various anti-inflammatories.<sup>1–3</sup> However, very limited pharmacological studies have been reported so far mainly because of the difficult in synthesis and the harsh reaction conditions. Due to the pharmacological potential of benzo[*c*]pyrazolo[1,2-*a*]cinnolin-1-ones, simple and easy methods are highly desirable.<sup>4</sup>

Heterogenization of the corresponding catalysts has become a significant tool to overcome various drawbacks, including catalyst recovery, product separation, environmental pollution and high reaction temperatures.<sup>5–8</sup> Along this line, the use of nanometals as catalysts has spread rapidly.<sup>9–13</sup> It has resulted in the development of several active and efficient nanocatalysts for various protocols that have several advantages over traditional catalysts such as superior activity and stability. The metal nanocatalysts can be immobilized on the support through two approaches. The first one is to deposit the presynthesized metal nanoparticles onto the support by chemical adsorption, which allows fine control over the size and shape of the metal nanoparticles. However, with this approach, the adsorbed nanocatalysts are easily leached from the support during the catalytic reaction. The other is approach is to directly grow metal nanoparticles on the support using the pregrafted organic functional molecules or polymers as a stabilizer. This method is much better for holding the metal nanoparticles. Periodic mesoporous organosilicas (PMOs) are from this class of functionalized ordered nanoporous materials. PMOs are synthesized by the simultaneous hydrolysis and condensation of alkoxysilane precursors bridged to organic groups in the presence of structure directing agents. PMOs can be easily recovered and reused in a typical chemical process.<sup>14–27</sup> Along this line, we prepared and developed metal containing organic-based periodic mesoporous organosilica materials and studied their catalytic

applications for synthesis of benzo[*c*]pyrazolo[1,2-*a*]cinnolin-1-ones. Continuing our research, we have replaced the organic groups with silica groups. Our study illustrated that APTPOSS was a powerful and highly efficient support for the successful immobilization and stabilization of the metal catalysts. Our goal was to enhance the strength of the catalyst structure by this replacement. This catalyst support functions *via* obstruction of KCC-1 by APTPOSS (APTPOSS@KCC-1). In fact, APTPOSS@KCC-1 is a nano labyrinth to hold the nanoparticle. We believe that this unique property will be very useful for the design of silica-supported catalysts, for which the accessibility of active sites can be increased significantly. This study aimed to develop novel catalysts and noble metal nanoparticles for the synthesis benzo[*c*]pyrazolo[1,2-*a*]cinnolin-1-ones by an eco-friendly method (Scheme 1). In this study, APTPOSS@KCC-1 was used as a new supporting material to stabilize Pd nanoparticles (Pd NPs) to obtain Pd/APTPOSS@KCC-1 nanocatalysts with enhanced accessibility for active sites and high surface area. We compared the three structures of APTPOSS@KCC-1, hyperbranched polyglycerol@KCC-1 (HPG@KCC-1), and ionic liquid@KCC-1 (IL@KCC-1) for the synthesis benzo[*c*]pyrazolo[1,2-*a*]cinnolin-1-one. APTPOSS@KCC-1 displayed not only suitable catalytic reaction rate but also excellent reusability in the catalytic reaction. The strong activity of this catalyst is attributed to its high accessibility and low probability of the aggregation and leaching of the nanoparticles on the APTPOSS@KCC-1 support system.

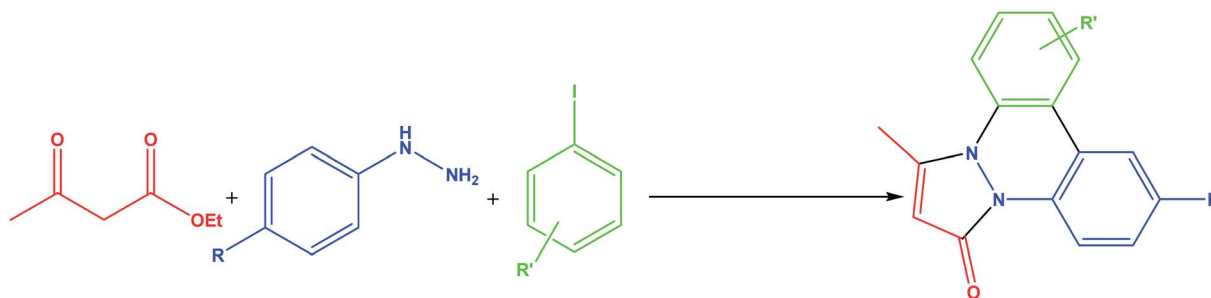
### Experimental

#### Materials and methods

Chemicals were purchased from Fluka and Merck. Melting points were determined in open capillaries using an Electro-thermal 9100 apparatus and are uncorrected. FTIR spectra were obtained by a VERTEX 70 spectrometer (Bruker) in the transmission mode in spectroscopic grade KBr pellets for all powders. The particle size and structure of nanoparticles were observed using a Philips CM10 transmission electron microscope operating at 100 kV. The content of phosphorous in the catalyst was determined by an OPTIMA 7300DV inductively

Department of Chemistry, Faculty of Sciences, Islamic Azad University Neyshabur Branch, Neyshabur, Iran. E-mail: [seyedmohsen.sadeghzadeh@gmail.com](mailto:seyedmohsen.sadeghzadeh@gmail.com); Fax: +98 561 2502065; Tel: +98 561 2502065





Scheme 1 Synthesis of benzo[c]pyrazolo[1,2-a]cinnolin-1-ones in the presence of Pd/X@KCC-1 (X = APTPOSS, HPG, and IL) NPs.

coupled plasma (ICP) analyzer. Powder X-ray diffraction data were obtained using a Bruker D8 Advance model with Cu K $\alpha$  radiation. Thermogravimetric analysis (TGA) was conducted on a NETZSCH STA449F3 at a heating rate of 10 °C min<sup>-1</sup> under nitrogen. <sup>1</sup>H and <sup>13</sup>C NMR spectra were obtained on a Bruker DRX-300 AVANCE spectrometer at 300.13 and 75.46 MHz and a Bruker DRX-400 AVANCE spectrometer at 400.22 and 100.63 MHz, respectively. Elemental analyses for C, H, and N were performed using a Heraeus CHN-O-rapid analyzer. The purity determination of the products and reaction monitoring were evaluated by TLC on silica gel polygram SILG/UV 254 plates. Mass spectra were obtained on a Shimadzu GCMS-QP5050 mass spectrometer.

#### General procedure for the preparation of KCC-1 nanoparticles

TEOS (2.5 g) was dissolved in a solution of cyclohexane (30 mL) and 1-pentanol (1.5 mL). A stirred solution of cetylpyridinium bromide (CPB 1 g) and urea (0.6 g) in water (30 mL) was then added. The resulting mixture was continually stirred for 45 min at room temperature and then placed in a Teflon-sealed hydrothermal reactor and heated 120 °C for 5 h. The silica formed was isolated by centrifugation, washed with deionized water and acetone, and dried in a drying oven. This material was then calcined at 550 °C for 5 h in air.

#### Preparation of ClPOSS nanoparticles

3-Chloropropyltrimethoxysilane (20 g), 450 mL of methanol and 22.5 mL of concentrated hydrochloric acid were mixed, and the mixture was stirred for at least 4 weeks at room temperature. Colourless crystals were obtained after being washed with water and dried in vacuum at 60 °C for 24 h.<sup>28</sup>

#### Preparation of octakis[3-(3-aminopropyltriethoxysilane)propyl]octasilsesquioxane (APTPOSS)

3-Aminopropyltriethoxysilane (20 mmol) and ClPOSS (2 mmol) were transferred to a reaction vessel under a nitrogen atmosphere, and the reaction solution was stirred at 100 °C for 2 days. Then, the mixture was cooled to room temperature, and the solution was filtered and washed with methanol and acetone.<sup>29</sup>

#### General procedure for the preparation of APTPOSS@KCC-1 nanoparticles

KCC-1 NPs (2 mmol) and THF (20 mL) were mixed together in a beaker, and then, NaH (20 mmol) was dispersed into the mixture by ultrasonication. APTPOSS (0.5 g) was added at room temperature and stirred for another 16 h at 60 °C. The resultant products were collected and washed with ethanol and deionized water and then dried under vacuum at 60 °C for 2 h for further use.

#### General procedure for the preparation of HPG@KCC-1 nanoparticles

KCC-1 NPs (2 mmol) were dispersed in a mixture of 80 mL of toluene and 1.0 mmol of potassium methylate (CH<sub>3</sub>OK), followed by the addition of 10 mL of anhydrous dioxane. Glycidol (2.0 g) was added dropwise over a period of 1 h. After vigorous stirring for 2 h, the final suspension was repeatedly washed, filtered for several times and dried at 60 °C in air.

#### General procedure for the preparation of IL@KCC-1 nanoparticles

KCC-1 NPs (2 mmol) and THF (20 mL) were mixed in a beaker, and then, NaH (20 mmol) was dispersed into the mixture by ultrasonication. 1,3-Bis(trimethoxysilylpropyl)imidazolium iodide (22 mmol) was added at room temperature and stirred for another 16 h at 60 °C. The resultant products were collected and washed with ethanol and deionized water and then dried under vacuum at 60 °C for 2 h for further use.

#### General procedure for the preparation of Pd/X@KCC-1 (X = APTPOSS, HPG, and IL) nanoparticles

A 100 mL round-bottom flask was charged with 0.5 g of X@KCC-1 nanocomposite, 0.1 g of Pd(OAc)<sub>2</sub> and 50 mL of acetonitrile, after which it was ultrasonically dispersed for 30 min. Subsequently, fresh NaBH<sub>4</sub> solution (0.2 M, 10 mL) was added dropwise into the abovementioned suspension. The product was isolated by centrifugation, washed repeatedly with deionized water and ethanol, and dried in a vacuum.

#### General procedure for the synthesis of benzo[c]pyrazolo[1,2-a]cinnolines

A mixture of ethyl acetoacetate (10 mmol), phenylhydrazine hydrates (10 mmol), aryl iodides (12 mmol), K<sub>2</sub>CO<sub>3</sub> (10 mmol),

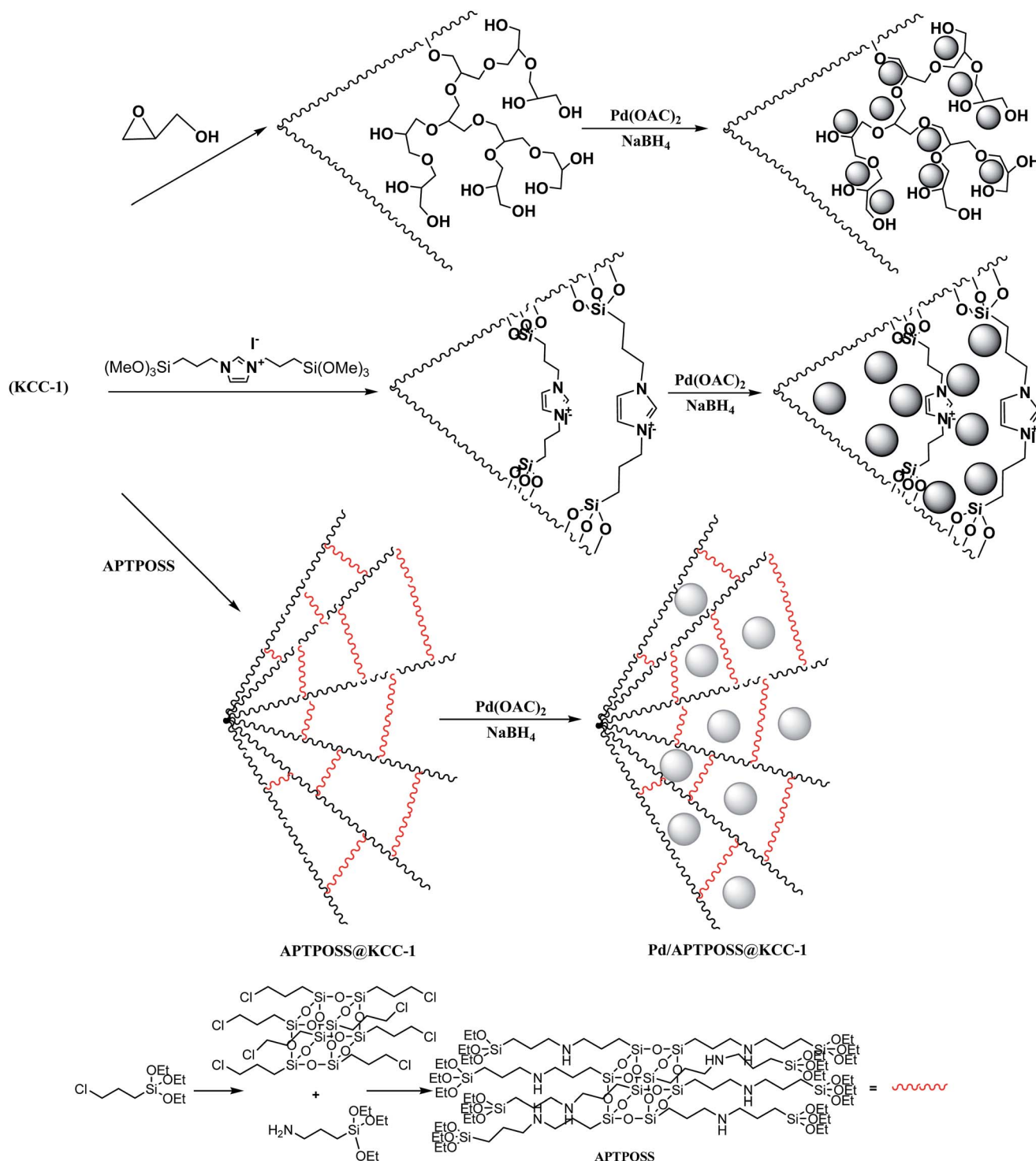


and Pd/X@KCC-1 (X = APTPOSS, HPG, and IL) NPs (12 mg) was stirred with heating under reflux in TFA (20 mL) for 2 hours. Then,  $K_2S_2O_8$  (1 mmol) was added consecutively. The mixture was stirred at room temperature for 10 min under  $N_2$  atmosphere and then heated under reflux for 6 h. The catalyst was separated by filtration. Evaporation of the solvent of the filtrate under reduced pressure gave the crude products. The pure

products were isolated by chromatography on silica gel eluted with petroleum ether : EtOAc (3 : 1).

## Results and discussion

Pd/X@KCC-1 (X = APTPOSS, HPG, and IL) were synthesized by a simple three step approach. In the first step, KCC-1 was



**Scheme 2** Schematic of the synthesis for Pd/X@KCC-1 (X = APTPOSS, HPG, and IL).



prepared by the simultaneous hydrolysis and condensation of tetramethoxysilane (TMOS). Then, the fibers of KCC-1 had many Si-OH groups on the surfaces; thus, it was expected that the KCC-1 could be easily functionalized with glycidol, APTPOSS, and 1,3-bis(trimethoxysilylpropyl)imidazolium iodide to form HPG@KCC-1, APTPOSS@KCC-1, and IL@KCC-1, respectively. Finally, hyperbranched polyglycerol, APTPOSS, and 1,3-bis(trimethoxysilylpropyl)imidazolium iodide groups on the X@KCC-1 (X = APTPOSS, HPG, and IL) could serve as aggregation centers for the growth of metal nanoparticles on the surface of KCC-1. We looked for the best combination of the three structure of APTPOSS, HPG, and IL to keep the nanoparticles in the context of KCC-1 (Scheme 2). This catalyst was then characterized with some techniques such as infrared (IR) spectroscopy, thermal gravimetric analysis (TGA), X-ray diffraction (XRD), transmission electron microscopy (TEM) and energy dispersive X-ray (EDX) spectroscopy. It can be noted that the authenticity of the synthesis of Pd/HPG@KCC-1 was mentioned in our previous the research.<sup>30</sup>

FT-IR spectroscopy was employed to determine the surface modification of the synthesized catalyst (Fig. 1). The SiO-Si symmetric and asymmetric stretching vibrations at  $802\text{ cm}^{-1}$  and  $1103\text{ cm}^{-1}$ , respectively, and the O-H stretching vibration at  $3444\text{ cm}^{-1}$  were observed for the KCC-1 (Fig. 1a). The bands observed at  $3121$  and  $2929\text{ cm}^{-1}$  are assigned to the C-H stretching of aromatic and aliphatic moieties, respectively. Moreover, the signals cleared at  $1563$  and  $1635\text{ cm}^{-1}$  are, respectively, attributed to C=C and C=N stretching vibrations of the imidazolium ring (Fig. 1b). These results indicated that the imidazolium IL had been successfully introduced onto the surface of KCC-1. The successful functionalization of the

APTPOSS based organic-inorganic hybrid on the KCC-1 surface is evidenced by two broad peaks at about  $1000\text{--}1150\text{ cm}^{-1}$ , assigned to Si-O stretching vibrations, as well as the presence of C-H stretching at  $2950\text{ cm}^{-1}$  and C-H bending vibration at approximately  $1450\text{ cm}^{-1}$  observed in Fig. 1c.

The XRD patterns of KCC-1 NPs, Pd/IL@KCC-1, and Pd/APTPOSS@KCC-1 NP catalyst are shown in Fig. 2. The broad peak between  $20^\circ$  and  $30^\circ$  corresponds to amorphous silica (Fig. 2a). Moreover, new peaks at  $2\theta = 40.1^\circ$ ,  $46.5^\circ$  and  $68^\circ$  reflection of the Pd (JCPDS 05-0681) (Fig. 2b) crystal were observed for Pd/APTPOSS@KCC-1, confirming the successful growth of Pd particles on the surface of APTPOSS@KCC-1 again. The broad peak between  $20^\circ$  and  $30^\circ$  corresponds to amorphous silica. XRD analysis can easily be indexed to the cubic phase of

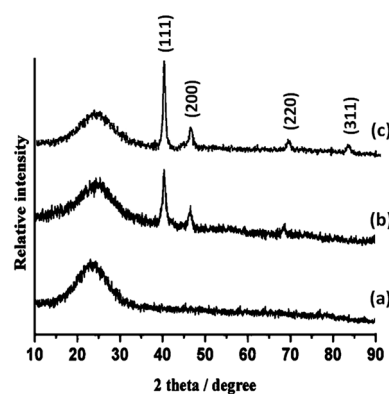


Fig. 2 XRD analysis of (a) KCC-1 NPs, (b) Pd/APTPOSS@KCC-1 NPs, (c) Pd/IL@KCC-1 NPs.

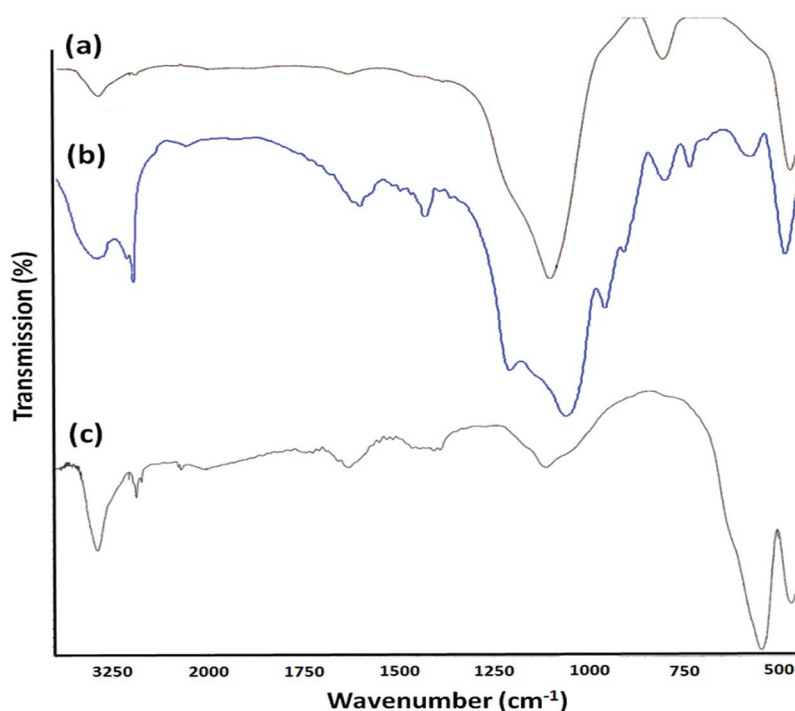


Fig. 1 FTIR spectra of (a) KCC-1 NPs, (b) Pd/IL@KCC-1 NPs, and (c) Pd/APTPOSS@KCC-1 NPs.



Pd NPs. Fig. 1c reveals that Pd NPs exhibit sharp peaks of Pd (111), Pd (200), Pd (220) and Pd (311), which also verify the existence of fcc-Pd, confirming the successful growth of metal particles on the surface of IL@KCC-1 again.

The structures of the synthesized Pd/IL@KCC-1 and Pd/APTPOSS@KCC-1 NPs were analyzed by TEM (Fig. 3). The as prepared KCC-1 microspheres with fibrous structure were uniform and monodispersed (Fig. 3). The average diameter of the microspheres was about 200–220 nm. TEM image shown in Fig. 3 further clarifies that the distance between the two fibers was about 10–15 nm. Moreover, after Pd was anchored, the metal nanoparticles are clearly distinguishable with the difference in their contrast. As can be observed, the as-prepared metal nanoparticles are spherical without obvious aggregation (Fig. 3a and b).

The  $N_2$  adsorption–desorption isotherms of Pd/X@KCC-1 (X = APTPOSS, IL, and HPG) showed characteristic type IV curve, which is consistent with literature reports on standard fibrous silica spheres (Fig. 4). For Pd/APTPOSS@KCC-1, Pd/IL@KCC-1, and Pd/HPG@KCC-1, the BET surface areas were 231, 238, and 195  $m^2 g^{-1}$ ; pore diameters were 11.26, 11.52, and 10.97 nm; and pore volumes 1.02, 0.98, and 0.87  $cm^3 g^{-1}$ , respectively. The nitrogen sorption analysis of Pd/APTPOSS@KCC-1 also confirms a regular and uniform mesostructure with a decrease in surface area, pore diameter and pore volume parameters in comparison with that of pristine KCC-1. With the functionalization by X-Si (X = APTPOSS, IL, and HPG), the corresponding pore volumes are drastically reduced. This could be ascribed to increased loading with the sensing probe, which occupies a large volume inside the silica spheres (Table 1).

The catalytic potential of the Pd/APTPOSS@KCC-1, Pd/IL@KCC-1, and Pd/HPG@KCC-1 NPs was evaluated in condensation reactions. At first, the reaction of ethyl acetoacetate (10 mmol), phenylhydrazine hydrate (10 mmol), and aryl iodide (12 mmol) was chosen as a model reaction to optimize the reaction conditions, such as the amount of catalyst, temperature, time, and solvent (Table 2). Applying 12 mg of catalyst in 50 mL TFA is the best conditions for the reaction. Moreover, it was found that conventional heating under reflux

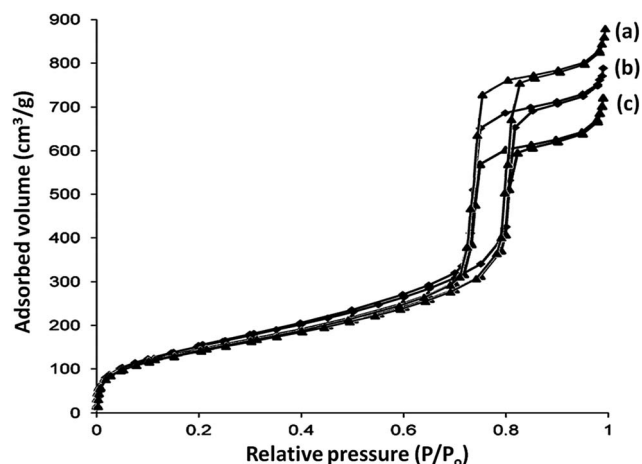


Fig. 4 Adsorption–desorption isotherms of (a) Pd/APTPOSS@KCC-1, (b) Pd/IL@KCC-1, and (c) Pd/HPG@KCC-1.

Table 1 Structural parameters of KCC-1 and Pd/X@KCC-1 (X = APTPOSS, IL, and HPG) materials determined from nitrogen sorption experiments

Catalysts	$S_{BET}$ ( $m^2 g^{-1}$ )	$V_t$ ( $cm^3 g^{-1}$ )	$D_{BJH}$ (nm)
KCC-1	439	1.49	14.78
Pd/APTPOSS@KCC-1	231	1.02	11.26
Pd/IL@KCC-1	238	0.98	11.52
Pd/HPG@KCC-1	195	0.87	10.97

for 8 h is more efficient. In all cases, higher catalyst power of Pd/IL@KCC-1 was evident relative to that of Pd/APTPOSS@KCC-1 and Pd/HPG@KCC-1. Reaction was conducted in a shorter time in the presence of the Pd/IL@KCC-1. This ability was due to the presence of ionic liquid on the catalyst structure. The ionic liquid may play the role of a catalyst in the reaction. Among the studied bases,  $K_2CO_3$  showed the best results for this reaction in terms of reaction time and yield and also  $K_2S_2O_8$  was the best oxidant for this reaction (Table 3).

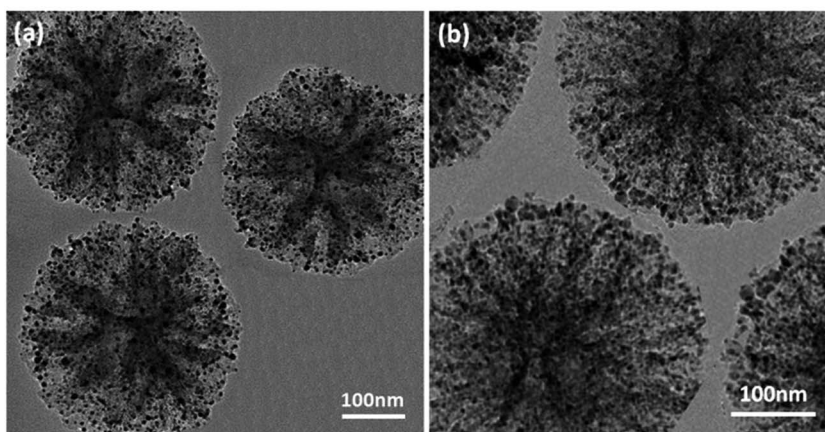


Fig. 3 TEM images of (a) Pd/APTPOSS@KCC-1 NPs and (b) Pd/IL@KCC-1 NPs.



**Table 2** Optimization of the reaction conditions for the synthesis of benzo[c]pyrazolo[1,2-a]cinnolin-1-ones in terms of temperature, solvent, time and product yield

Entry	Catalyst	Solvent	Temp. (°C)	Time (h)	Yield <sup>a</sup> (%)
1	Pd/APTPOSS@KCC-1	—	100	8	—
	Pd/IL@KCC-1				—
	Pd/HPG@KCC-1				—
2	Pd/APTPOSS@KCC-1	TFA	Reflux	8	87
	Pd/IL@KCC-1				91
	Pd/HPG@KCC-1				88
3	Pd/APTPOSS@KCC-1	EtOH	Reflux	8	51
	Pd/IL@KCC-1				39
	Pd/HPG@KCC-1				53
4	Pd/APTPOSS@KCC-1	H <sub>2</sub> O	Reflux	8	45
	Pd/IL@KCC-1				31
	Pd/HPG@KCC-1				46
5	Pd/APTPOSS@KCC-1	CH <sub>2</sub> Cl <sub>2</sub>	Reflux	8	64
	Pd/IL@KCC-1				67
	Pd/HPG@KCC-1				62
6	Pd/APTPOSS@KCC-1	<i>n</i> -Hexane	Reflux	8	—
	Pd/IL@KCC-1				—
	Pd/HPG@KCC-1				—
7	Pd/APTPOSS@KCC-1	TFA	60	8	74
	Pd/IL@KCC-1				80
	Pd/HPG@KCC-1				75
8	Pd/APTPOSS@KCC-1	TFA	40	8	—
	Pd/IL@KCC-1				—
	Pd/HPG@KCC-1				—
9	Pd/APTPOSS@KCC-1	TFA	Reflux	7	84
	Pd/IL@KCC-1				90
	Pd/HPG@KCC-1				85
10	Pd/APTPOSS@KCC-1	TFA	Reflux	6	72
	Pd/IL@KCC-1				90
	Pd/HPG@KCC-1				71
11	Pd/APTPOSS@KCC-1	TFA	Reflux	5	68
	Pd/IL@KCC-1				86
	Pd/HPG@KCC-1				65
12	Pd/APTPOSS@KCC-1	TFA	Reflux	8	87
	Pd/IL@KCC-1				91
	Pd/HPG@KCC-1				88
13	Pd/APTPOSS@KCC-1	TFA	Reflux	8	76
	Pd/IL@KCC-1				91
	Pd/HPG@KCC-1				78
14	Pd/APTPOSS@KCC-1	TFA	Reflux	8	67
	Pd/IL@KCC-1				85
	Pd/HPG@KCC-1				69

<sup>a</sup> Isolated yields.

To assess the exact impact of the presence of APTPOSS in the catalyst, Pd/APTPOSS@KCC-1 was compared with Pd/IL@KCC-1 and Pd/HPG@KCC-1. The loading amount of Pd in Pd/APTPOSS@KCC-1, Pd/IL@KCC-1, and Pd/HPG@KCC-1 was determined by inductively coupled plasma (ICP). The amount of Pd in Pd/APTPOSS@KCC-1 was less than the amount of Pd/HPG@KCC-1, but it is almost equal with that of Pd/IL@KCC-1. This amount was reused for ten consecutive cycles of catalysis, and the amount of Pd in Pd/APTPOSS@KCC-1, Pd/IL@KCC-1 and Pd/HPG@KCC-1 was stable. However, this amount was reduced by half in KCC-1. The abilities of the Pd/APTPOSS@KCC-1, Pd/IL@KCC-1, and Pd/HPG@KCC-1 are attributed to APTPOSS, IL, and HPG units that effectively manage the reaction by preventing Pd agglomeration and

releasing and recapturing Pd during the reaction process. It is interesting that the amount of Pd in Pd/APTPOSS@KCC-1 was stable after being reused for twenty cycles, wherein a significant reduction in the amount of Pd in Pd/HPG@KCC-1 and Pd/IL@KCC-1 was observed. This remarkable ability of the Pd/APTPOSS@KCC-1 mesostructure may be attributed to stability of coupling APTPOSS and KCC-1 (Table 4). To examine this matter, the loading amount of HPG and IL in the fresh Pd/HPG@KCC-1 and Pd/IL@KCC-1 after twenty reuses was determined by TGA. The amount of HPG and IL in Pd/HPG@KCC-1 and Pd/IL@KCC-1 after twenty reuses was about half that of the fresh Pd/HPG@KCC-1 and Pd/IL@KCC-1, but the amount of APTPOSS in Pd/APTPOSS@KCC-1 was equal to the fresh Pd/APTPOSS@KCC-1 (Fig. 5).



**Table 3** Optimization of the reaction conditions for the synthesis of benzo[c]pyrazolo[1,2-a]cinnolin-1-ones in the presence of different oxidants and bases

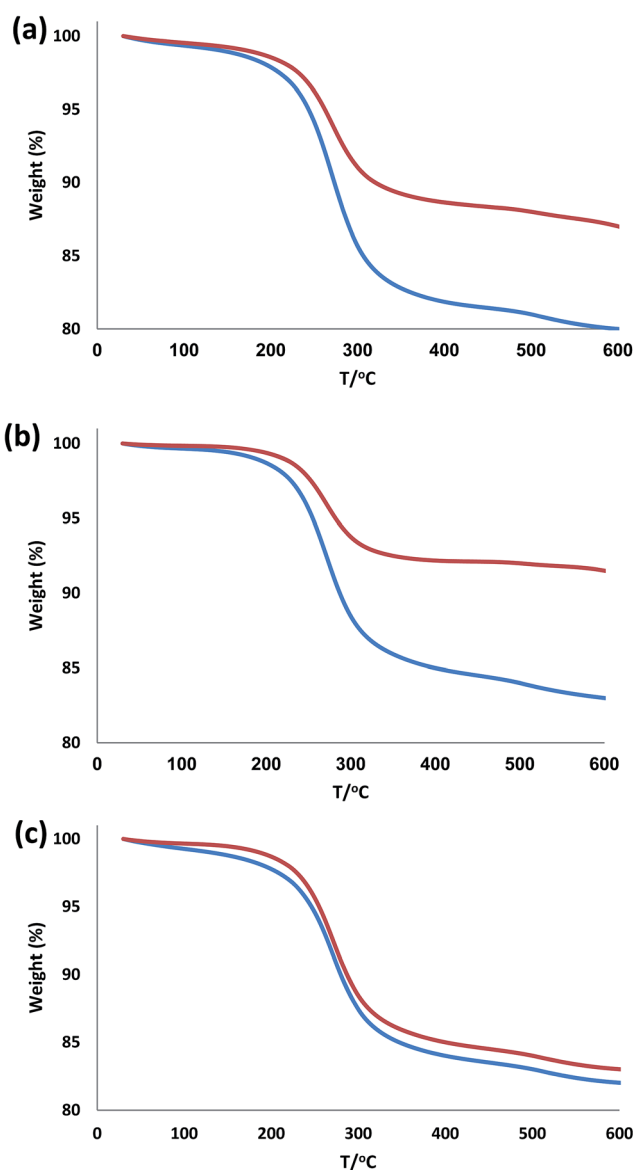
Entry	Catalyst	Base	Oxidant	Yield <sup>a</sup> (%)
1	Pd/APTPOSS@KCC-1	K <sub>2</sub> CO <sub>3</sub>	K <sub>2</sub> S <sub>2</sub> O <sub>8</sub>	87
	Pd/IL@KCC-1			91
	Pd/HPG@KCC-1			88
2	Pd/APTPOSS@KCC-1	K <sub>2</sub> CO <sub>3</sub>	—	—
	Pd/IL@KCC-1			—
	Pd/HPG@KCC-1			—
3	Pd/APTPOSS@KCC-1	K <sub>2</sub> CO <sub>3</sub>	AgOAc	60
	Pd/IL@KCC-1			61
	Pd/HPG@KCC-1			58
4	Pd/APTPOSS@KCC-1	K <sub>2</sub> CO <sub>3</sub>	Ag <sub>2</sub> O	48
	Pd/IL@KCC-1			53
	Pd/HPG@KCC-1			46
5	Pd/APTPOSS@KCC-1	K <sub>2</sub> CO <sub>3</sub>	Cu(OAc) <sub>2</sub>	54
	Pd/IL@KCC-1			52
	Pd/HPG@KCC-1			53
6	Pd/APTPOSS@KCC-1	K <sub>2</sub> CO <sub>3</sub>	(NH <sub>4</sub> ) <sub>2</sub> S <sub>2</sub> O <sub>8</sub>	32
	Pd/IL@KCC-1			35
	Pd/HPG@KCC-1			37
7	Pd/APTPOSS@KCC-1	—	K <sub>2</sub> S <sub>2</sub> O <sub>8</sub>	—
	Pd/IL@KCC-1			—
	Pd/HPG@KCC-1			—
8	Pd/APTPOSS@KCC-1	CsF	K <sub>2</sub> S <sub>2</sub> O <sub>8</sub>	38
	Pd/IL@KCC-1			45
	Pd/HPG@KCC-1			37
9	Pd/APTPOSS@KCC-1	Na <sub>2</sub> CO <sub>3</sub>	K <sub>2</sub> S <sub>2</sub> O <sub>8</sub>	74
	Pd/IL@KCC-1			70
	Pd/HPG@KCC-1			72
10	Pd/APTPOSS@KCC-1	Et <sub>3</sub> N	K <sub>2</sub> S <sub>2</sub> O <sub>8</sub>	84
	Pd/IL@KCC-1			90
	Pd/HPG@KCC-1			85
11	Pd/APTPOSS@KCC-1	NaOAc	K <sub>2</sub> S <sub>2</sub> O <sub>8</sub>	68
	Pd/IL@KCC-1			66
	Pd/HPG@KCC-1			65
12	Pd/APTPOSS@KCC-1	KOH	K <sub>2</sub> S <sub>2</sub> O <sub>8</sub>	36
	Pd/IL@KCC-1			39
	Pd/HPG@KCC-1			37
13	Pd/APTPOSS@KCC-1	K <sub>3</sub> PO <sub>4</sub>	K <sub>2</sub> S <sub>2</sub> O <sub>8</sub>	39
	Pd/IL@KCC-1			37
	Pd/HPG@KCC-1			40
14	Pd/APTPOSS@KCC-1	Cs <sub>2</sub> CO <sub>3</sub>	K <sub>2</sub> S <sub>2</sub> O <sub>8</sub>	52
	Pd/IL@KCC-1			55
	Pd/HPG@KCC-1			48

<sup>a</sup> Isolated yields.

To further understand this issue, we compared TEM images of used catalyst with those of the fresh catalyst. Comparison of TEM images of used catalyst (Fig. 6) with those of the fresh catalyst (Fig. 3) showed that the morphology and structure of Pd/X@KCC-1 (X = APTPOSS, IL, and HPG) NPs remained intact after twenty recoveries. Fig. 6 shows degradation of the structure of Pd/HPG@KCC-1 and Pd/IL@KCC-1 in the reuse process, but the amount of degradation was more in Pd/IL@KCC-1 (Fig. 6a and b). However, the functionalization of the Pd/APTPOSS@KCC-1 NPs does not result in the change of the morphology (Fig. 6c). This study proves that the stabilities of the structures of Pd/APTPOSS@KCC-1 NPs were due to the presence

**Table 4** The loading amount of nano palladium in Pd/APTPOSS@KCC-1, Pd/IL@KCC-1, and Pd/HPG@KCC-1 NPs

Entry	Catalyst	Reuse wt%		
		1	10	20
1	Pd/KCC-1	4.3	2.2	0.9
2	Pd/HPG@KCC-1	6.2	5.9	1.9
3	Pd/IL@KCC-1	5.7	5.1	2.7
4	Pd/APTPOSS@KCC-1	5.9	5.8	5.5

**Fig. 5** TGA diagram of (a) Pd/HPG@KCC-1, (b) Pd/IL@KCC-1, and (c) Pd/APTPOSS@KCC-1. (Blue) new catalyst. (Red) recovered catalyst.

of APTPOSS in the catalyst structure. APTPOSS can be a strong scaffold in the KCC-1 structure.

With the optimized reaction conditions in hand, we next managed to examine the scope and limitation of this palladium



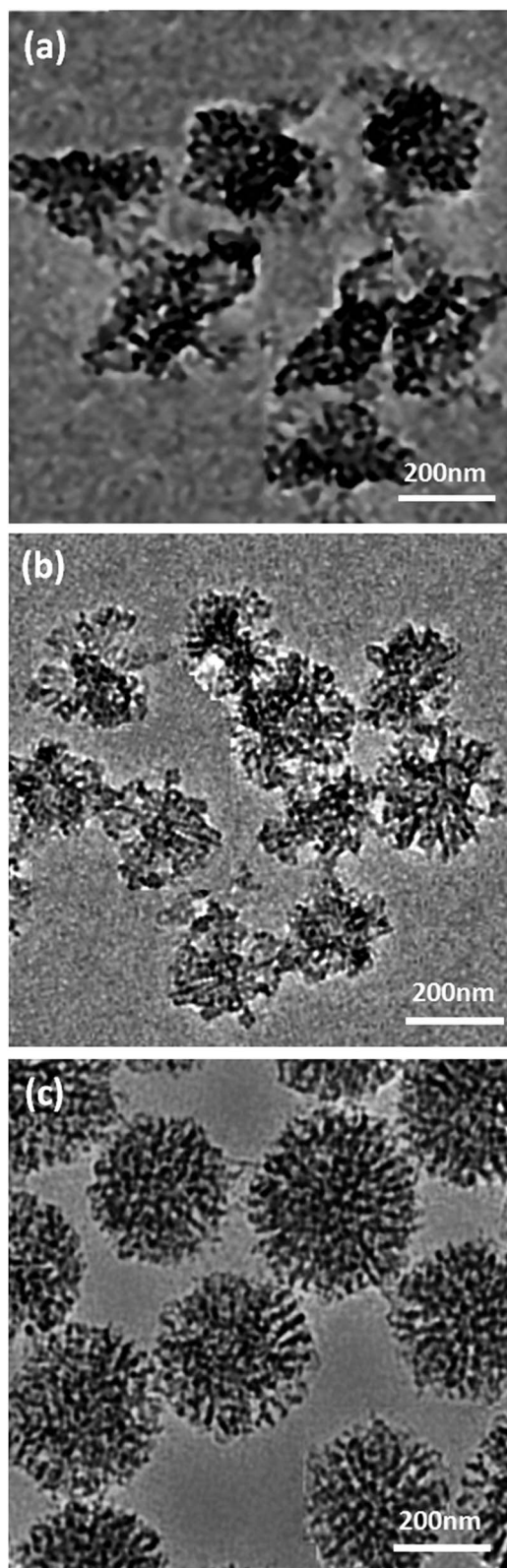


Fig. 6 TEM images of (a) Pd/IL@KCC-1 NPs, (b) Pd/HPG@KCC-1 NPs, and (c) Pd/APTPOSS@KCC-1 NPs after ten reuses.

cross-coupling reaction with various types of phenylhydrazine hydrates and aryl iodides. The results of this study are collected in Table 5. As can be seen from Table 5, electronic effects and

Table 5 Synthesis of benzo[c]pyrazolo[1,2-a]cinnoline of various phenylhydrazine hydrates and aryl iodides with ethyl acetoacetate in the presence of Pd/APTPOSS@KCC-1 NPs<sup>a</sup>

Entry	Phenylhydrazine hydrate	Aryl iodide	Time (h)	Yield <sup>b</sup> (%)
1			8	87
2			8	82
3			10	79
4			9	81
5			9	85
6			8	80
7			9	80
8			8	86
9			10	84
10			10	77
11			10	75

<sup>a</sup> Reaction conditions: ethyl acetoacetate (10 mmol), phenylhydrazine hydrates (10 mmol), aryl iodides (12 mmol), K<sub>2</sub>CO<sub>3</sub> (10 mmol), K<sub>2</sub>S<sub>2</sub>O<sub>8</sub> (10 mmol) and Pd/HPG@KCC-1 NPs (12 mg) were stirred with heating under reflux in TFA (30 mL) for 8–10 hours. <sup>b</sup> Isolated yields (%).

the nature of substituents on the phenylhydrazine hydrates and aryl iodides did not show strong obvious effects in terms of yields under the reaction conditions. Phenylhydrazine hydrates



Table 6 The reusability of catalysts for synthesis of benzo[c]pyrazolo[1,2-a]cinnoline

Catalyst	Recycle																			
	1	2	3	4	5	6	7	8	9	10	11	12	13	14	15	16	17	18	19	20
Pd/APTPOSS@KCC-1	87	87	87	87	87	87	87	87	86	86	86	86	86	86	86	86	85	85	85	85
Pd/IL@KCC-1	91	91	90	90	90	89	87	85	85	85	80	74	69	63	58	52	47	41	36	28
Pd/HPG@KCC-1	88	88	88	86	83	81	78	75	71	67	65	60	58	54	49	47	43	39	36	32
Pd/KCC-1	64	59	52	50	47	41	39	35	34	30	29	29	27	24	21	18	17	17	14	12

and aryl iodides containing electron-withdrawing groups or electron-donating groups were employed and reacted well to give the desired products in good yields with high purity.

The recovery and reuse of a catalyst is highly preferable for a catalytic process. Our goal since the development of silica was the production of a new support with high power in recovery and reuse. After ten reuse cycles from Pd/KCC-1, the catalyst performance decreased by half, and after twenty, this amount was below twenty percent. To solve this problem, functionalization was achieved by post-synthetic modification of the fibers of KCC-1 by reaction with IL and HPG to produce IL@KCC-1 and HPG@KCC-1, which could then act as pseudochelators or ligands to control the metal leaching during the reaction. After twenty consecutive reuses, the IL@KCC-1 and HPG@KCC-1 could not give a satisfactory catalytic activity under mild reactions. After ten reuse cycles from IL@KCC-1 and HPG@KCC-1, the catalyst performance fell between 30% and 40%. Based on these frustrating results, we continued the research to improve the yield of the product by adding the APTPOSS to the catalyst. Pd/APTPOSS@KCC-1 NPs exhibited catalytic activity almost identical to that of the fresh catalyst (Table 6). The reason for this difference in yield was the designed and synthesized APTPOSS functionalized KCC-1. Moreover, the blockage of pore entrances by APTPOSS could also account for the decreased leaching of nanoparticles.

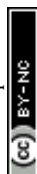
## Conclusions

In this study, a novel fibrous KCC-1 based Pd/APTPOSS@KCC-1 nanocatalyst with high surface area and significantly increased accessibility of the active sites was successfully synthesized. The main development in this study was adding APTPOSS to the structure of KCC-1, which increases the power of the KCC-1 substrate to keep the nanocatalyst. Thus, Pd NPs were remarkably well dispersed on the fibers of the KCC-1 microspheres without aggregation. The Pd/APTPOSS@KCC-1 nanocatalyst exhibited excellent catalytic activity in its synthesis of benzo[c]pyrazolo[1,2-a]cinnolines, which may be attributed to the high accessibility of the KCC-1 support material and the low amount of aggregation of the Pd NPs on the Pd/APTPOSS@KCC-1 support. Furthermore, Pd/APTPOSS@KCC-1 can be reused at least ten times without an obvious reduction in catalytic activity. This is partially due to the prevention of leaching of Pd NPs from the fibrous support. Moreover, the blockage of pore entrances by APTPOSS could also account for the decreased leaching of Pd NPs. Thus, the study of the APTPOSS@KCC-1 nanocatalyst may provide a potential platform for the

fabrication of other noble metal nanocatalysts with easy accessibility, which would be highly efficient in various noble metal based catalytic reactions. This process may be used in the future to develop additional nanocatalysts that possess favorable properties such as efficiency and ease of reuse.

## Notes and references

- 1 E. Andre, A. Georges and A. Serge, *C. R. Seances Acad. Sci., Ser. C*, 1967, **264**, 1855.
- 2 E. Andre and I. Georges, *Bull. Soc. Chim. Fr.*, 1964, **11**, 2897.
- 3 E. Andre and P. Rene, *Bull. Soc. Chim. Fr.*, 1962, 292.
- 4 Z. Fan, K. Wu, L. Xing, Q. Yao and A. Zhang, *Chem. Commun.*, 2014, **50**, 1682–1684.
- 5 M. Benaglia, *Recoverable and Recyclable Catalysts*, John Wiley & Sons, Chichester, 2009.
- 6 S. Wittmann, A. Shatz, R. N. Grass, W. J. Stark and O. Reiser, *Angew. Chem., Int. Ed.*, 2010, **49**, 1867–1870.
- 7 C. Coperet, M. Chabanas, R. P. Saint-Arroman and J. M. Basset, *Angew. Chem., Int. Ed.*, 2003, **42**, 156–181.
- 8 J.-M. Basset, C. Coperet, D. Soulivong, M. Taoufik and J. Thivolle-Cazat, *Acc. Chem. Res.*, 2010, **43**, 323–334.
- 9 M. Garcia-Melchor, M. C. Pacheco, C. Najera, A. Lledos and G. Ujaque, *ACS Catal.*, 2012, **2**, 135–144.
- 10 A. L. Isfahani, I. Mohammadpoor-Baltork, V. Mirkhani, A. R. Khosropour, M. Moghadam, S. Tangestaninejad and R. Kia, *Adv. Synth. Catal.*, 2013, **355**, 957–972.
- 11 Y. P. Shang, X. M. Jie, J. Zhou, P. Hu, S. J. Huang and W. P. Su, *Angew. Chem., Int. Ed.*, 2013, **52**, 1299–1303.
- 12 H. Kamisaki, T. Nanjo, C. Tsukano and Y. Takemoto, *Chem.–Eur. J.*, 2011, **17**, 626–633.
- 13 H. Li and J. J. Cooper-White, *Nanoscale*, 2013, **5**, 2915–2920.
- 14 Q. Yang, J. Liu, L. Zhang and C. Li, *J. Mater. Chem.*, 2009, **19**, 1945–1955.
- 15 F. Hoffmann and M. Fröba, *Chem. Soc. Rev.*, 2011, **40**, 608–620.
- 16 M. S. Moorthy, S.-S. Park, D. Fuping, S.-H. Hong, M. Selvaraj and C.-S. Ha, *J. Mater. Chem.*, 2012, **22**, 9100–9108.
- 17 U. Díaz, D. Brunel and A. Corma, *Chem. Soc. Rev.*, 2013, **42**, 4083–4097.
- 18 A. P. Wight and M. E. Davis, *Chem. Rev.*, 2002, **102**, 3589–3614.
- 19 A. Stein, *Adv. Mater.*, 2003, **15**, 763–775.
- 20 B. Hatton, K. Landskron, W. Whitnall, D. Perovic and G. A. Ozin, *Acc. Chem. Res.*, 2005, **38**, 305–312.
- 21 F. Hoffmann, M. Cornelius, J. Morell and M. Fröba, *Angew. Chem., Int. Ed.*, 2006, **45**, 3216–3251.



- 22 S. Fujita and S. Inagaki, *Chem. Mater.*, 2008, **20**, 891–908.
- 23 S. El Hankari, B. Motos-Pérez, P. Hesemann, A. Bouhaouss and J. J. E. Moreau, *Chem. Commun.*, 2011, **47**, 6704–6706.
- 24 M. Waki, N. Mizoshita, T. Tani and S. Inagaki, *Angew. Chem., Int. Ed.*, 2011, **50**, 11667–11671.
- 25 B. Karimi, D. Elhamifar, O. Yari, M. Khorasani, H. Vali, J. H. Clark and A. J. Hunt, *Chem.–Eur. J.*, 2012, **18**, 13520–13530.
- 26 D. Elhamifar, B. Karimi, J. Rastegar and M. H. Banakar, *ChemCatChem*, 2013, **5**, 2218–2224.
- 27 D. Elhamifar and A. Shábani, *Chem.–Eur. J.*, 2014, **20**, 3212–3217.
- 28 U. Dittmar, B. J. Hendan, U. Flörke and H. C. Marsmann, *J. Organomet. Chem.*, 1995, **489**, 185–194.
- 29 J. Safaei-Ghomi, S. H. Nazemzadeh and H. Shahbazi-Alavi, *Appl. Organomet. Chem.*, 2016, **30**, 911–916.
- 30 S. M. Sadeghzadeh, *Catal. Sci. Technol.*, 2016, **6**, 1435–1441.

